Carbon Dot-Sensitized Photoanodes for Visible Light-Driven Organic Transformations

*Francisco Yarur Villanueva, John Manioudakis, Rafik Naccache, Marek B. Majewski**

Department of Chemistry and Biochemistry and Centre for NanoScience Research, Concordia University, Montreal, QC, Canada, H4B 1R6.

KEYWORDS Zinc oxide, carbon dots, solar energy conversion, catalysis, nanomaterials

ABSTRACT Visible light photosensitization of metal oxides to create heterostructures for the conversion of solar-to-chemical energy is a promising approach to produce solar fuels and other valuable chemicals. Carbon dots have recently been considered as suitable candidates to sensitize wide bandgap metal oxide semiconductors due to their low cost and tunable optical properties. While photocatalytic systems using carbon dots as sensitizers have been reported, transformations involving the production of value-added chemicals as well as the electron transfer mechanisms underpinning photocatalysis within such heterostructures remain underexplored. Here we report the sensitization of zinc oxide nanowires with carbon dots for the α-heteroarylation of 1-phenylpyrrolidine with 2-chlorobenzothiazole under visible light illumination at room temperature. The carbon dots improve the light absorption of the nanowires in the visible region of the spectrum affording the use of white light to drive catalysis. From optical spectroscopy and electrochemistry investigations of the resulting nanohybrid material, the photocatalytic properties are explained by the band alignment at the zinc oxide-carbon dot junction where a series of single electron transfers creates the necessary potential to oxidize 1-phenylpyrrolidine. The resulting cascade of electron transfers into and from the carbon dots drives the α-heteroarylation to a 97% yield after 24 hrs.

Introduction

Coupling reactions that involve heteroaromatic compounds and amines are a key component in the synthesis of organic semiconductors,[1, 2] anion exchange membrane fuel cells,[3] and pharmaceuticals.[4] Photocatalytic devices engineered from Earth-abundant elements that can drive such reactions are an inexpensive alternative to traditional methods in synthetic organic chemistry and, therefore, highly desired. Heterogeneous photocatalytic surfaces such as nanostructured semiconducting metal oxides, although more difficult to study with respect to mechanism elucidation are typically stable and readily recyclable.[5] Furthermore, heterogeneous photoredox systems are comparable in performance with molecular ones; however, they have the advantage of being easily extractable from solution.[6] For these catalysts to be industrially viable, they must be simple and economical to prepare/operate relative to well-established synthetic methodologies (e.g. palladium mediated cross-coupling reactions).[7-9] Many photocatalytic mechanisms in organic synthesis leverage the inherent reactivity of oxygen species and other radicals.[10, 11] For instance, Stache *et al*. have activated C-O bonds through a photocatalytic mechanism using $[Ir(dFMeppy)_2(dtbbpy)][PF_6]$ [dFMeppy = 2-(2,4-difluorophenyl)-5-methylpyridine, dtbbpy = 4,4′-di-tert-butyl-2,2′-bipyridine] via the generation of phosphoranyl radicals.[12] In another illustrative example, Cai *et al.* have made use of a graphitic-C_3N_4 photocatalyst to generate α-tertiary and α-secondary aminoalkyl radicals, in high yield, as precursors for different organic transformations.[13] Nonetheless, these radical driven reactions have some drawbacks, including long reaction times, sensitizer photobleaching, unwanted by-products, and mass transfer limitations between the radical and the substrate.[14, 15] Camussi *et al.*, showed how a g-C_3N_4 photocatalyst can sensitize $^1O_2$ to drive cycloaddition reactions albeit with low chemoselectivity due to two proposed mechanisms with which $^1O_2$ could react with the

substrates.[16] Acknowledging these limitations, and by employing lessons learned from the design of materials for solar fuels generation, we envisioned that it should be possible to drive clean and chemoselective coupling reactions with a photoelectrode (acting as a heterogeneous photocatalyst) in an air-free environment to generate valuable products in high yield.

Many semiconducting materials have been explored to drive solar energy conversion including metal oxides,[17] sulfides,[18] and organic polymers.[19] Few, if any, of these materials fully meet the requirements to maximize the absorption of sunlight (e.g. narrow band gap, low cost, long-term stability, and minimal pathways for charge recombination).[20] Zinc oxide nanowires (NWs) have emerged as promising materials for these photoelectrochemical applications because of their shortened charge carrier collection pathways, large surface area, and charge-steering capabilities.[21, 22] However, ZnO has a wide bandgap (3.37 eV) limiting the absorption of visible light and subsequently, the quantum efficiency.[23] To increase the incident photon to converted electron (IPCE) ratio, developing new ways of sensitizing ZnO nanomaterials to absorb wavelengths in the visible portion of the solar spectrum is of particular interest.

Efforts have been devoted to the sensitization of ZnO NWs through doping, attachment of plasmonic structures, and dye and quantum dot sensitization.[24-26] Kadi *et al.* have previously doped ZnO NWs with fluorine in order to decrease the bandgap energy of the material and to further employ the resulting device as a heterogeneous catalyst for the photodegradation of malachite green dye using visible light.[27] Guo *et al*. have sensitized ZnO NWs with graphene quantum dots to perform water splitting,[28] and Lee *et al.* have coupled a ruthenium-based dye to ZnO in order to increase the absorption of light throughout the visible spectrum (in a strategy analogous to those employed in dye sensitized solar cells).[29] Although these sensitization

methods vary in their degree of efficiency, some of the aforementioned sensitizers are costly while others make use of heavy metals which are significantly harder to recycle.[30]

Recently, carbon dots (CDs) have emerged as candidates for various applications due to their low cost and chemical toxicity, optical properties, and stability.[31-33] The implementation of CDs for light-conversion applications as a new generation of photosensitizers has also increased as a result of their high photostability and tunable light absorption.[34, 35] Moreover, these nanomaterials have shown photocatalytic activity for the degradation of organic contaminants, water splitting/hydrogen production, and the redox catalysis of different organic reactions to produce high value-added chemicals by visible light.[36-38] The latter has been relatively underexplored with greater focus on the degradation of organic dyes likely owing to the logistical simplicity regarding reaction monitoring and product isolation/characterization.[39, 40] In a marriage of the two materials discussed (*vida supra*), we anticipate that the surface functionalization of ZnO NWs with CDs will open new avenues for the engineering and development of "green" nanohybrid devices.[28, 41, 42] To date, the design of such devices is partially hindered by fast electron-hole recombination kinetics,[43] device stability,[44] low quantum yields,[45] and a general lack of understanding about the molecular processes occurring at the interface of such heterogeneous photoelectrodes.[40]

Here, we report the fabrication of a metal oxide-carbon dot nanohybrid photoelectrode for the photocatalytic α-heteroarylation of tertiary amine 1-phenylpyrrolidine (**1**) and the production of a high value-added benzylic amine pharmacophore (Scheme 1) as well as offer insight into possible mechanisms of electron transfer between the photoelectrode and organic substrate. The photoelectrode is formed via the growth of ZnO NWs on a fluorine-doped tin oxide (FTO) on glass substrate through a hydrothermal reaction and subsequent functionalization with previously

unreported visible light absorbing carbon dots prepared from citric acid and propylenediamine (**PD2-CDs**) through attachment of anchoring surface groups on the **PD2-CDs**. The photoelectrodes prepared in this fashion exhibit an enhanced photocurrent under visible light irradiation and a further increase upon exposure to tertiary amines.

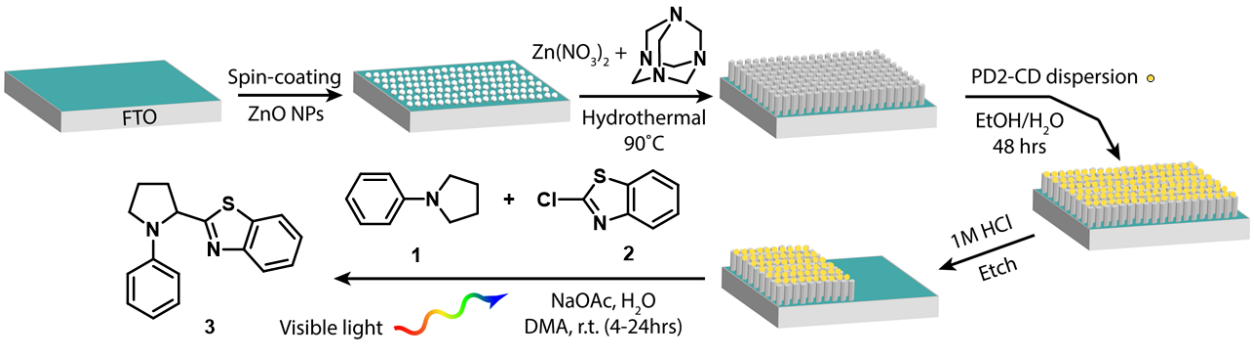

Scheme 1. Fabrication protocol for the photoelectrodes described in this work along with the proposed reaction scheme for the α-heteroarylation of 1-phenylpyrrolidine (1) with 2-chlorobenzothiazole (2) via irradiation of a carbon dot functionalized ZnO NW photoelectrode.

Experimental

Materials

Zinc chloride ($ZnCl_2$), zinc nitrate hexahydrate [$Zn(NO_3)_2 \cdot 6H_2O$], hexamethylenetetramine (HMTA), linoleic acid, sodium hydroxide (NaOH), citric acid, propylenediamine (PD2), glutathione, formamide, and fluorine doped tin oxide (FTO) on glass were purchased from Sigma-Aldrich and used as received. Tetrabutylammonium hexafluorophosphate ($TBAPF_6$) was purchased from Tokyo Chemical Industry Co. (TCI) and recrystallized three times from ethanol (99%) before use. 1-Phenylpyrrolidine (**1**) and 2-chlorobenzothiazole (**2**) were purchased from

Alfa Aesar and used without further purification. *N,N*-Dimethylacetamide (DMA) was purchased from Fisher Scientific and used as received.

General procedures

Transmission electron microscopy (TEM) images were collected using a benchtop LVEM5 microscope from Delong Instruments (Brno, Czech Republic) operating at 5 kV for the ZnO NPs and a JEM-2100F (Jeol Ltd) analytical electron microscope operating under 200 kV for the **PD2-CDs**. Three 2 µL aliquots of a 500 µg mL^{-1} ZnO NP dispersion in 95% ethanol were pipetted onto a Cu-300HD grid (Pacific Grid-Tech). **PD2-CDs** were also casted onto Cu-300HD grids by immersing the grid in a 1 mg mL^{-1} dispersion in 18 MΩ water. Images were processed using Fiji imaging software where the ZnO NP size was determined (average of ca. 200 particles). The morphology of the ZnO NWs was characterized through scanning electron microscopy (SEM) using a FEI Quanta 3D FEG Dual Beam instrument working at 5 kV. The films were sputter-coated with Pt before all measurements.

A K-Alpha X-ray photoelectron spectrometer (Thermo Scientific) in standard lens mode was used to obtain the XPS spectra of the PD2-CDs. A 400 mm spot size was analyzed using a CAE analyser with a 50.0 eV pass energy and a 0.100 eV energy step. The measurements were performed in triplicate with 10 runs for each scan. The average of the triplicates was used to plot both the survey and the HR spectra.

Powder X-ray diffraction (PXRD) measurements were performed using a 2nd Gen D2 Phaser X-ray diffractometer with monochromatized Cu Kα radiation with a nickel filter (Bruker AXS). The X-ray source was set to a power of 30 kV and 10 mA in a continuous PSD fast scan mode. Diffraction patterns were recorded in 2θ ranging from 20 to 70° with a step increment of 0.05°

and scan speed of 1 s step^{-1} with a PSD opening of 4.7970°. The data analysis was performed with XPert Highscore software.

Attenuated Total Reflectance (FTIR-ATR) analysis was performed using a Thermo Scientific Nicolet iS5 equipped with an iD5 ATR accessory. The spectra were acquired in 64 scans, with a resolution of 0.4 cm^{-1}, a gain of 1, an optical velocity of 0.4747 cm s^{-1}, and an aperture setting of 100. The Omic 9 software package was used to process the raw data. UV-Visible absorption spectra were obtained from 200-800 nm using a Cary 5000 Series UV-Vis-NIR Spectrophotometer (Agilent Technologies) and a 1 cm quartz cuvette or a film sample holder. A 5.0 nm bandwidth with a wavelength changeover at 350 nm and a scan speed of 600 nm s^{-1} with a resolution of 1 nm were used for analysis. Diffuse reflectance spectroscopy (DRS) spectra were collected from 350-800 nm using a Cary 6000 Series UV-Vis-NIR spectrophotometer (Agilent Technologies) coupled with an integrating sphere. A 5.0 nm bandwidth with a wavelength changeover at 350 nm and a scan speed of 600 nm s^{-1} with a resolution of 1 nm were used for analysis. Photoelectrode thickness was analyzed using a Dektak XT contact profilometer with a stylus force of 10 mg.

Electrochemical measurements were performed on a WaveDriver 200 Integrated Bipotentiostat/Galvanostat workstation (Pine Research Instrumentation, Inc.). A three-electrode system was employed to measure the photoelectrochemical response of ZnO NW films as a working electrode (WE) with a platinum wire as a counter electrode (CE) and a Ag/AgCl (3 M KCl) reference electrode (RE) in 0.1 M KOH solution. All potentials were measured against the reference electrode. ZnO films without functionalization were irradiated with a 4 W UV lamp (λ_{ex} = 365 nm) at a distance of ca. 10 cm. The electrochemical properties of the **PD2-CDs** were determined using a three-electrode system by drop-casting **PD2-CDs** from 95% ethanol onto a

platinum button WE (2 mm diameter) with a platinum wire as a CE and a Ag wire pseudo-reference electrode in 0.1 M $TBAPF_6$ in acetonitrile. All potentials were referenced against ferrocene as an internal standard.

Photocatalysis

All photocatalysis measurements were performed in a homemade photoreactor setup. In a representative procedure, a glass vessel loaded with 1-phenylpyrrolidine (**1**, 276 μL, 1.875 mmol), 2-chlorobenzothiazole (**2**, 163 μL, 1.25 mmol), sodium acetate (205 mg, 1 mmol), H_2O (18 MΩ, 225 μL, 2.5 mmol) and a stir bar was sparged with argon for 10 min. DMA (5 mL) was transferred into a vial under argon and sonicated for 45 min while bubbling argon. Subsequently, the solvent was transferred to the reaction vessel with a three-electrode setup (the film acting as the WE), to monitor the photocurrent produced over the course of the reaction. This vessel was placed on a stir plate and inside a homebuilt photoreactor with four white light LEDs (Cree XP-G3 Cool White) for 4–24 hrs. A fan was placed on top of the reactor to maintain the reaction temperature at ca. 23 °C (see Supporting Information, Figure S1). The product of the reaction was isolated and purified as described in the Supporting Information.

Synthesis of zinc oxide nanowires (ZnO NWs)

NWs were synthesized from zinc nitrate hexahydrate and HMTA in a hydrothermal reaction by a procedure optimized in our lab (see Supplementary Information). Five fluorine-doped tin oxide (FTO) on glass substrates (ca. 2 cm × 1 cm) were first cleaned by immersing them separately in soapy water (10 min), distilled water (10 min), and 95% ethanol (10 min) under sonication. The cleaned substrates were dried in an oven at 80 °C for at least 4 hours prior to deposition and then were spin-coated (3×, 1500 rpm, 2 s) with two drops of a dispersion of ZnO

NPs (see Supporting Information) in 95% ethanol (1 mg mL^{-1}). After the casting process, the slides were placed upside down inside a centrifuge tube for the addition of the growing solution. An aliquot of aqueous $Zn(NO_3)_2 \cdot 6H_2O$ solution (17 mL, 0.13 M) was combined with aqueous HMTA (13 mL, 0.2 M) and transferred to the centrifuge tube containing the ZnO NP substrates. The tube was left in an oven at 90 °C for 3 hrs for the NWs to grow on the slides. Then, the sides were rinsed thoroughly with distilled water and 95% ethanol and left to air dry for further experiments.

Carbon dot synthesis (PD2-CDs)

The **PD2-CDs** were synthesized through the hydrothermal reaction of citric acid and propylenediamine (PD2). Citric acid (0.960 g, 500 mmol) and PD2 (0.320 mL, 375 mmol) were added to 10 mL of water in a hydrothermal reactor. The solution was heated to 210 °C for a period of 4 hrs with stirring at 300 rpm. The product was a dark brown solution which was subjected to dialysis for 5 days in Milli-Q water, using a 1 kDa MWCO dialysis bag (Spectra/Por®6 RC – Spectrum Laboratories), and changing the water every 24 hrs to remove the unreacted material. Then, the sample was placed in an oven at 70 °C overnight to concentrate it to ~5 mL, followed by three organic washes with 40 mL of acetone (99%) to further purify the **PD2-CDs**. Once the **PD2-CD** solution was concentrated, 40 mL of acetone was added, the sample was vortexed for 30 s and centrifuged at room temperature at 10 kG for 10 min. The supernatant was discarded, and two more acetone washes were performed on the sample. It is important to note that the fluorescence of the supernatant was evaluated after every wash to make sure the sample was free from any impurities and unreacted fluorophores. By the third wash the fluorescence of the supernatant was insignificant, meaning that the product is pure. The

purified product was dried in an oven at 80 °C overnight, crushed into a fine powder and dispersed in water or 95% ethanol for further experiments.

ZnO NW|PD2-CD film preparation

The **ZnO NW|PD2-CD** heterostructures were prepared by a simple reaction in ethanolic solution. In a typical procedure, two films of ZnO NWs were placed in a 50 mL beaker, immersed in a dispersion of **PD2-CDs** (7 mL, 150 μL mL^{-1}), and covered by aluminum foil. The dispersion of **PD2-CDs** was prepared by adding 525 μL of a 2 mg mL^{-1} dispersion of **PD2-CDs** in Milli-Q water (18 MΩ) to 6.5 mL of 95% ethanol. The films were left in this dispersion under constant stirring for a period of 48 hrs for the **PD2-CDs** to attach and cover the whole surface. Additionally, after the reaction period the films were rinsed thoroughly with 95% ethanol to remove any unattached **PD2-CDs** and left to air dry. Finally, one edge of the film was immersed in a 1 M HCl solution to etch and normalize the active surface of the film to ca. 1.5 cm^2. The films were rinsed with 95% ethanol and left to air dry in the dark prior to further analysis.

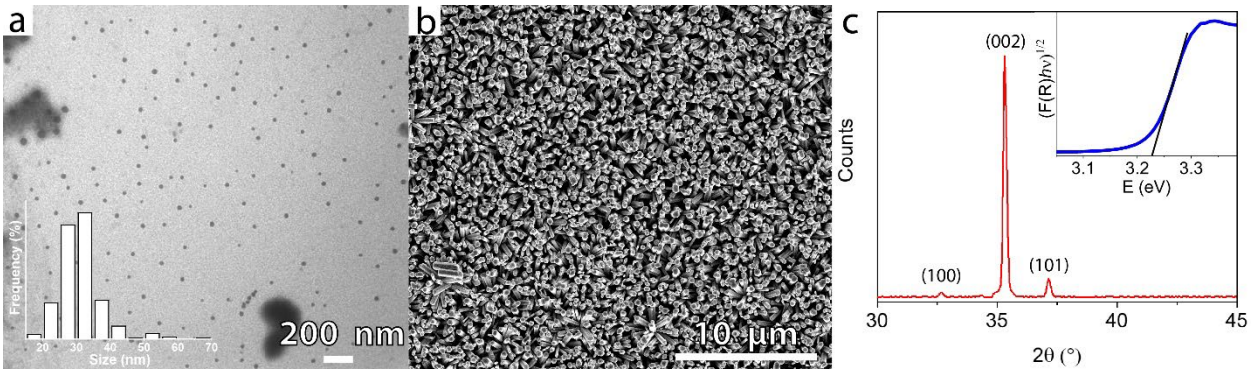

Figure 1. a) TEM micrograph of the ZnO NPs. b) SEM micrograph of the ZnO NWs grown on an FTO substrate. The image depicts highly oriented wires with hexagonal heads and a low degree of

aggregation. c) PXRD spectrum for the ZnO NW films on FTO. The preferred orientation for the growth is observed through the (002) plane as this peak is significantly greater than the ones for the other phases. (c, inset) Diffuse reflectance spectrum plotted using the Kubelka-Munk function.

Results and discussion

The ZnO NWs were prepared by spin-coating a ZnO NP dispersion onto an FTO on glass slide, followed by hydrothermal reaction of $Zn(NO_3)_2 \cdot 6H_2O$ and HMTA at 90 °C. From transmission electron microscopy (TEM) investigations (Figure 1a), the ZnO NPs used as seeds for nanowire growth are spherical and monodisperse with an average size of 32 ± 4.7 nm. The crystallinity of the NPs was evaluated through powder X-ray diffraction (PXRD) which shows crystalline reflections for the (100), (002), (101), (102), (110), (103), and (112) planes (Figure S2) in agreement with previously reported values.[46] Scanning electron microscopy (SEM) of the as-grown ZnO NWs shows highly oriented and tightly packed hexagonal wires with a calculated average diameter of 130 ± 28.2 nm (Figure 1b). These wires produce films of an average thickness of 1.3 μm as measured by profilometry. The PXRD pattern for the NWs (Figure 1c) displays characteristic peaks for wurtzite ZnO: (100), (101), and a prominent (002) signal corresponding to the preferred orientation of the nanowires on the surface.[47] The bandgap of this semiconductor film was calculated to be 3.22 eV from the band edge of the diffuse reflectance spectrum (DRS; inset Figure 1c).

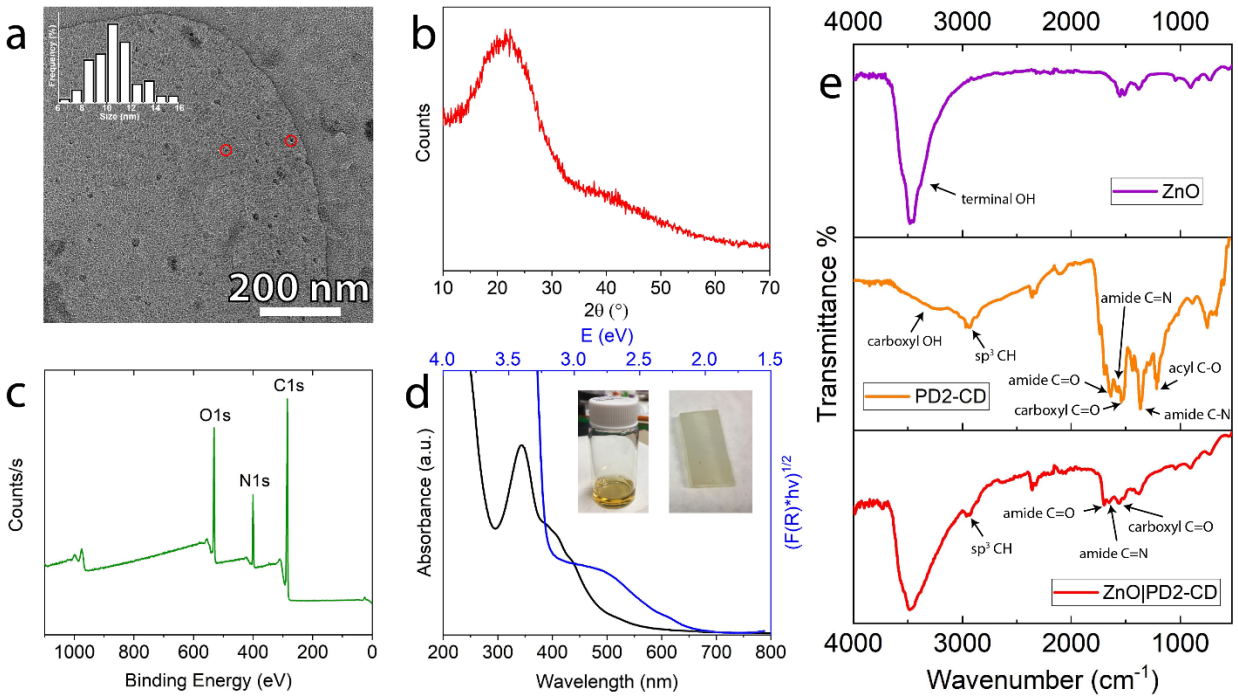

Figure 2. a) TEM spectrograph of the PD2-CDs with two representative carbon dots highlighted (red circles). b) PXRD diffractogram for the PD2-CDs in powder form, which confirms the amorphous nature of the material. c) XPS survey scan indicating the presence of carbon, nitrogen and oxygen. d) UV-vis (black trace) spectrum and Kubelka-Munk plot (blue trace) for PD2-CDs dispersed in water and the functionalized films, respectively. The Kubelka-Munk plot corroborates the presence of PD2-CDs on the films with a broad peak that extends from 2.0 to 2.75 eV. d, inset) Ethanolic solution of PD2-CDs used for film functionalization and a ZnO NW film after exposure to the PD2-CD solution. e) FTIR spectra for the ZnO NWs (top), PD2-CDs (middle), and ZnO NW|PD2-CD scraped from the substrate (bottom). The functionalized film displays bands for the alkyl -CH and amide bond stretches over the ZnO bands, which further confirms the attachment of the PD2-CDs onto the films.

The **PD2-CD** photosensitizers were synthesized from citric acid and propylenediamine in a hydrothermal reaction effectively highlighting the low cost and simplicity of the synthesis of this

class of nanomaterials.[48, 49] We expect these starting materials to yield CDs that are N-doped, where heteroatom doping in CDs is considered to be a form of passivation to enhance the optical properties of the material.[34, 50] The presence of amide groups in CDs has previously been shown to increase the quantum yield of emission in this family of nanoparticles.[51] TEM analysis (Figure 2a) of the prepared and purified **PD2-CDs** shows an average size of 10.7 ± 1.5 nm. PXRD analysis (Figure 2b) confirms the amorphous nature of the **PD2-CDs** and the X-ray photoelectron spectroscopy (XPS) survey scan (Figure 2c) shows three different binding energies: 285, 400, and 531 eV, which correspond to C1s, N1s, and O1s, respectively. These data correlate with the expected CD elemental composition from citric acid and propylenediamine. The data extracted from high resolution XPS (HR-XPS) spectra were assigned to the respective bonds in the **PD2-CDs**, where the deconvolution for C1s (Figure S3a) shows the presence of C-C/C=C (284.3 eV), C-O (286.3 eV), and C-N/C=O (287.6 eV) bonds; for N1s (Figure S3b), the deconvolution shows two peaks corresponding to N-C/N-C (399.8 eV), and N-O (402.3 eV) bonds; and for O1s (Figure S3c) the spectra can be deconvoluted into two binding energies representing C=O (530.7 eV), and C-OH/C-O-C (531.8 eV) bonds. The elemental composition of the **PD2-CDs** was extracted from the HR-XPS by comparing the integrated peak areas for C, N and O and was found to be 71.95%, 11.61%, and 16.45%, respectively. The ability to optimize the optical properties of CDs based on the materials they are synthesized from to maximize the absorption of light in the visible part of the spectrum is of particular interest, and the absorption spectrum of the **PD2-CDs** (Figure 2d) in an aqueous dispersion shows a maximum absorption peak centered at 352 nm and a wide shoulder that extends deep into the visible region (from ca. 380 to 550 nm). The maximum at λ_{abs} = 352 nm is attributed to a $\pi \rightarrow \pi^*$ transition, while the shoulder is assigned to the $n \rightarrow \pi^*$ transition from the aromatic sp^2 domains of the C=O and

C=N bonds, respectively.[52] The Fourier transform infrared (FTIR) spectrum of the **PD2-CDs** (Figure 2e) shows bands between 3500-3000 cm^{-1} corresponding to -OH surface groups, as well as stretching modes at 2977 cm^{-1} for alkyl C-H groups, 1632 and 1532 cm^{-1} for amide and carboxyl C=O groups, 1556 cm^{-1} for amide C=N, 1364 cm^{-1} for the C-N, and 1213 cm^{-1} for acyl C-O (Table S1).

Attachment between the ZnO NWs and the **PD2-CDs** was achieved by immersing the NW films in an ethanolic dispersion of **PD2-CDs** for 48 hrs. After the attachment process the color of the films changed from white to pale orange (Figure 2d, inset). Optical characterization of the sensitized films by diffuse reflectance spectroscopy shows that the electronic properties of the pristine ZnO NWs are unaffected by the addition of the **PD2-CDs** as the bandgap absorption edge at 3.22 eV can still be observed (Figure 2d) while a significant increase in visible light absorption is observed, stemming from a broad band that extends from 2.0 to 2.75 eV. These values correlate to the optical bandgap values for the **PD2-CDs** in water (Figure 2d). In addition, diffuse reflectance FTIR spectroscopy (DRIFTS) confirms the presence of the **PD2-CDs** on the ZnO NWs where the stretch for the amide group can be distinguished at 1700 cm^{-1} (Figure S4). To determine the nature of the interaction between the **PD2-CDs** and ZnO NWs, FTIR spectroscopy on material scraped from the functionalized films (Figure 2e) was carried out. The broad band between 3600 to 3100 cm^{-1} is attributed to terminal -OH bond stretching, which becomes broader once the **PD2-CDs** are adsorbed onto the film. FTIR spectra for both the **PD2-CDs** alone and the **PD2-CDs** with the NWs show a band for the alkyl C-H stretch at 2971 and 2933 cm^{-1} confirming the presence of the **PD2-CDs** on the film. The band centered at 1562 cm^{-1}, assigned to the C=O stretch of the amide shifts from 1532 cm^{-1} in the free CDs. The band centered at 1378 cm^{-1} for the C-N bond also exhibits a shift from 1364 cm^{-1}. These fluctuations

in the stretching vibrations can be correlated to the change in the dielectric environment between the solvated **PD2-CDs** in a water dispersion and rigidified on ZnO.[53] The attachment of different functional groups to the surface of ZnO nanomaterials has been well documented in the literature through experimental and computational methods.[54] Carboxyl groups usually have a tight binding mode to ZnO according to computational studies where this functional group coordinates via two asymmetric bonds between the -COOH oxygens.[55, 56] Likewise, -SH and -NH_2 groups are also known to bind to ZnO.[54]

Cyclic voltammetry was used to estimate the HOMO/LUMO energies of the **PD2-CDs** (Figure 3a). When the potential was scanned through the oxidative side, two oxidative waves were observed; a non-reversible wave with an onset value of E_{ox} = +1.1 V (all potentials reported versus NHE) and one with an onset potential of E_{ox} = +1.6 V. Conversely, once the reductive side of the cyclic voltammogram was analyzed, a wave with a reductive onset of E_{red} = −2.4 V was observed. These values suggest a HOMO-LUMO gap of 3.5 eV (352 nm) which correlates to the absorption peak from the UV-Vis of the **PD2-CDs** dispersed in water (λ_{max} = 342 nm).

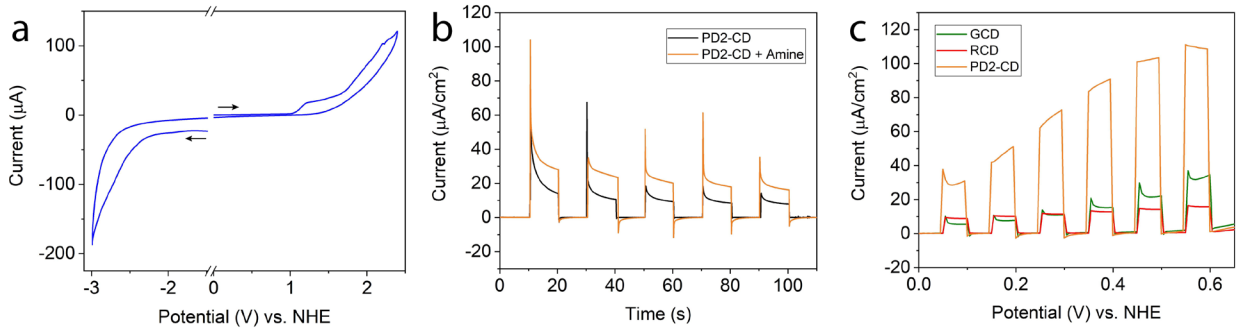

Figure 3 a) Cyclic voltammograms for the calculation of the HOMO and LUMO positions from both the non-reversible peak and the oxidative onset potential and from the reductive onset

potential, respectively. b) Chronoamperograms of the chopped-light experiment with white LEDs on the films with (orange trace) and without (black trace) **1**. c) Linear sweep voltammograms comparing the electrochemical behavior of different types of CDs (**GCD** and **RCD**) with the **PD2-CDs** used in this study (orange trace) upon 1-phenylpyrrolidine addition. RE: Ag wire; CE: Pt wire; WE: **ZnO NW|PD2-CD** film, 0.1 M $TBAPF_6$ in dimethylformamide (Scan rate: 100 mV s^{-1}).

The photocurrent of the nanostructured ZnO NW photoelectrode was first characterized using chronoamperometry (CA) in a three-electrode system before taking measurements on the sensitized films to confirm the semiconducting properties of the composite material. These photocurrent measurements were performed under chopped UV light illumination (λ_{ex} = 365 nm) in a 0.1 M solution of KCl without any sacrificial agents (Figure S5). A current increase and a capacitive effect due to the build-up of charges at the solid-liquid interface was observed on irradiation. Chopped-light chronoamperometry with no applied bias was also used to investigate the production of photocurrent over time upon white light irradiation of the **ZnO NW|PD2-CD** films (Figure 3b). There is a clear current increase on irradiation which suggests the injection of electrons from the excited state of the **PD2-CDs** into the conduction band of the ZnO NWs according to the proposed band alignment of the LUMO (−2.44 V) of the **PD2-CDs** and the literature value for the conduction band of ZnO (−0.3 V).[57] In this regard, the ZnO NWs are acting as a support and stabilizer of the reduced **PD2-CDs** and as a sink for reducing equivalents, harvesting electrons that could then be used in follow-on single electron transfer (SET) processes. The stability of the connection between the **PD2-CDs** and the NWs was evaluated by performing five chopped-light chronoamperometric experiments on a **ZnONW|PD2CD** film.

Each experiment was performed in a fresh electrolyte solution and the photocurrent was recorded upon white light illumination (Figure S6). It was observed that the current density diminishes to 70% of its original value in the fifth solution and after being exposed to 25 on-off illumination cycles (Table S2). Thus, we conclude that the interaction between the NWs and the **PD2-CDs** must be of a reasonable strength for the **PD2-CDs** to inject electrons into ZnO, surviving multiple solvent exchange and light irradiation cycles.

The oxidation of 1-phenylpyrrolidine (**1**) by the ground state of the **PD2-CDs** is feasible based on the predicted electron injection mechanism established from the calculated position of the HOMO level for the **PD2-CDs** (Step 1, Scheme 2) and the oxidation potential of the **1** (Figure S7). From our data, we estimate that SET from 1-phenylpyrrolidine (**1**) to the HOMO of the **PD2-CD** (Step 1, Scheme 2) is energetically feasible ($\Delta G° = -0.14$ kcal mol^{-1}, Eqn. S1). Such an electron transfer would create a radical centered on the nitrogen of the tertiary amine while replenishing the ground state of the **PD2-CD** which can be leveraged as an oxidant ($E_{ox} = +1.1$ V).

Considering that the energetics of our photoelectrode are well understood, we proceeded to evaluate the photocatalytic behavior of **ZnO NW|PD2-CDs** towards the photooxidation of **1**. The photocurrent observed upon white light irradiation of the films increases after the addition of one drop of **1** into the electrolyte solution in comparison to the photocurrent observed without the amine in solution (Figure 3b). This rise in current can be explained by the single electron photooxidation of **1** by the oxidized **PD2-CDs** on the ZnO surface, (Step 1, Scheme 2). We anticipate that the charge carrier density of the ZnO NWs would not only be increased by injection of electrons originating on the **PD2-CDs** themselves, but also from the subsequent replenishment of the **PD2-CD** ground state by **1**, thus producing an increase in current passing

through the film. The need for an applied bias was evaluated via the photooxidative performance of the CDs upon the addition of **1** with respect to a linear sweep voltammetry (Figure 3c) experiment. For contrast, the **PD2-CDs** reported here were compared to two other types of visible-light absorbing CDs (**GCDs** and **RCDs**, Figs. S8, S9 and Table S3) to see which CD system would be competent to drive the photooxidation of **1**. **GCDs** were synthesized from glutathione and formamide, thus, functional groups including carboxylic acids, amines, amides, and thiols are expected to be found on the surface,[58] while the **RCDs** (previously unreported), were prepared by reacting citric acid and formamide to yield mainly carboxylic acid and amine groups on the carbon dot surface (Figure S9). Therefore, these somewhat different surface environments are expected to create variations in the excited state redox potentials of the CDs, along with imparting them with different optical properties. Surprisingly, the **PD2-CDs** significantly outperformed the other two types of CDs, despite the other CDs having clear absorption maxima in the visible region (Figure S8), allowing them to harvest more visible light, while the **PD2-CDs** only have a shoulder that extends into the visible region. There was no photooxidation observed for the **RCDs** even at high potentials and we observed minimal photooxidation by the **GCDs** starting at a potential of +0.35 V. Conversely, the **PD2-CDs** used in our device showed significant photooxidation of **1** at virtually no applied bias. Therefore, an organic transformation using the oxidized form of **1** should be plausible by employing this film as a heterogeneous photocatalyst. From our analysis, all the CDs reported here are capable of oxidizing **1** from their respective excited states, somewhat at odds with what we observed in the LSV (Figure 3c). One possible explanation for the increased catalytic performance of the PD2-CDs is related to matching the emission of the LEDs used in our photocatalytic experiments and the absorbance maxima of the different CDs (Figure S10). We note that the blue emission

component of the LEDs aligns well with the absorption shoulder of the **PD2CDs**, increasing the number of available excited states to drive the formation of the radical of **1**. Somewhat significantly, this comparison demonstrates the flexibility and tunability of CDs for solar energy conversion purposes. By simply varying the starting materials of CD synthesis or by surface treatment one can achieve different optical and electronic properties that can be tailored to catalyze specific transformations.[59, 60]

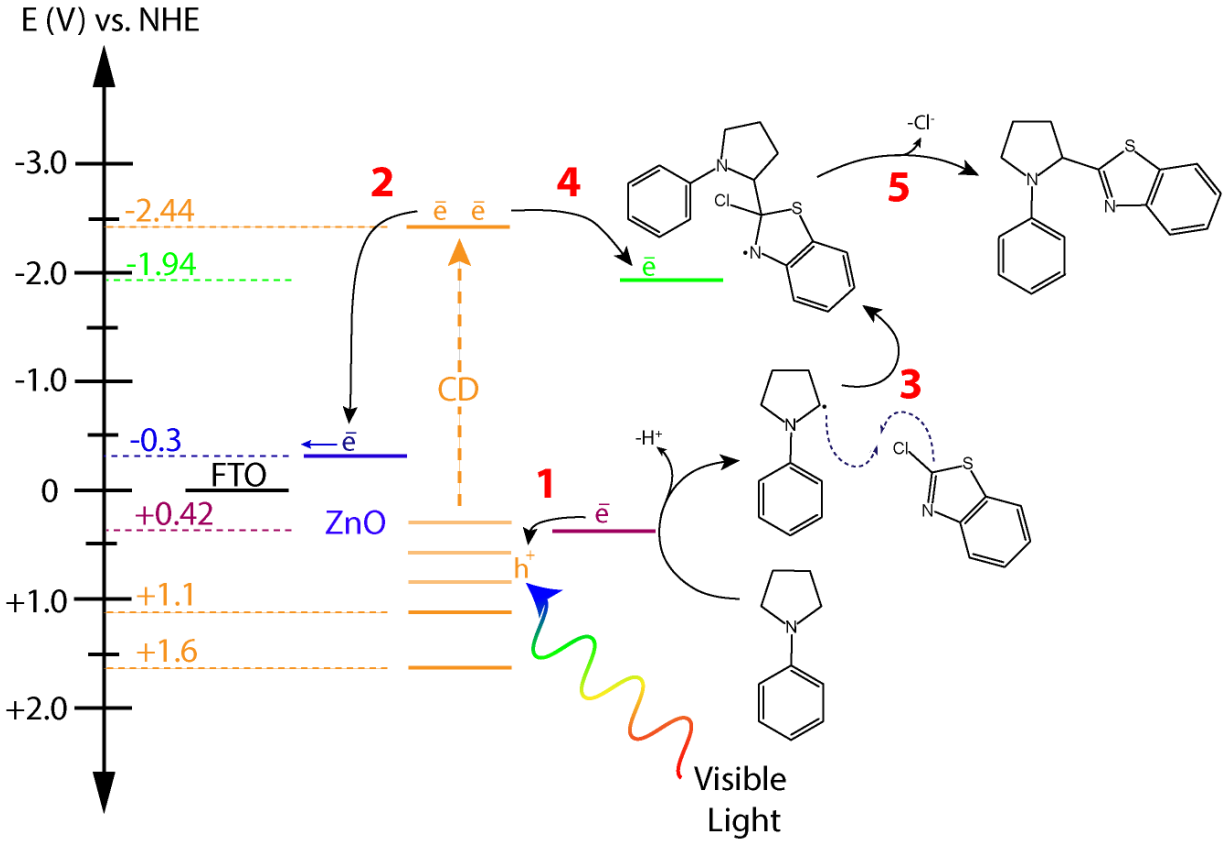

Scheme 2. Proposed reaction scheme and suggested mechanism for the photocatalytically driven reaction of 1-phenylpyrrolidine (1) and 2-chlorobenzothiazole (2) with the respective redox potentials for the active species.

Coupling heteroaromatic molecules to the α-carbon position of tertiary amines is an interesting catalytic conversion due to the generation of high value-added products, particularly in the pharmaceutical industry.[61-63] Considering the importance of these transformations in the production of relevant medicinal drugs,[64-66] they have been rather underexplored. With this in mind, we decided to catalyze a direct α-heteroarylation of **1** and **2** using the **ZnO NW|PD2-CD** photoelectrodes. To our knowledge, this photocatalytic transformation has only been reported twice by the same group employing a molecular iridium photocatalyst and obtaining yields of 75-87% depending on the reaction conditions.[67, 68] Prier and MacMillan performed the direct α-heteroarylation of different amines using $[Ir(ppy)_2(dtbbpy)][PF_6]$ (ppy = 2-phenylpyridine), where they promoted a mechanism that avoids the use of cyanoarenes and the associated radical anion pathway. Our photocatalytic system is expected to follow the same mechanistic steps while replacing the molecular catalysts with a heterogeneous photocatalyst created from Earth-abundant elements as the key components of the system. Since the reaction conditions have previously been optimized by Prier *et al.* we decided to employ the highest yield conditions and optimize them for our catalytic system.[67]

The reaction of **1** and **2** was performed in an inert atmosphere by mixing the starting materials with sodium acetate and water in dimethylacetamide (DMA) and exposing this solution to the film and white light irradiation at room temperature. As reported in Table 1 (Entry 5), the highest yield was obtained after 24 hrs (97% yield). However, film degradation was observed beginning at approximately 10 hrs into the reaction period, likely due to an increasing HCl concentration over the course of the reaction and/or photocorrosion of the ZnO NWs.[69] Therefore, 10 hrs was established as an optimal reaction time to yield significant product while preserving the integrity of the films (Table 1 Entry 2) as confirmed by DRIFTS and SEM of the films pre- and post-

reaction (Figures S4 and S11). The recyclability of the films was evaluated by performing the reaction for 10 hrs, rinsing the used film thoroughly, and using it for another 10 hr reaction period. On the second reaction we observed a yield of 55%. As expected, our device does not provide satisfactory results for a reaction that produces higher concentrations of acid as a by-product, highlighting one key area for optimization in future devices. The reaction was monitored through a bulk electrolysis (BE) experiment with no applied bias and UV-Vis spectroscopy in order to monitor the kinetics of the transformation. The current versus time plot (Figure S12) shows that there is a notable increase in charge density over the course of the first 30 min of the reaction, followed by stabilization after 1 hr. We postulate that this rapid initial current increase is due to the efficient oxidation of **1** through a SET process involving the **PD2-CDs** on the surface of the NWs (Step 1, Scheme 2) and a subsequent buildup of the radical product. Analysis of the UV-Vis spectra (Figure S13) over the course of the reaction reveals that product **3** is generated at a steady rate following zero-order kinetics, which is expected for heterogeneous catalysts where the reactants saturate the active surface.[70] Additionally, the initial generation and successive buildup of the 1-phenylpyrrolidine radical was also investigated through UV-Vis (Figure S14). In this case, the reaction was conducted without the addition of **2** and showed a rapid decrease in the concentration of **1** in the first fifteen minutes of reaction followed by a slow and stable consumption, which correlates with the current observed in the BE experiment. The oxidation of the amine is accompanied by the deprotonation of the α-C-H bond, which shifts the radical to the α-C (Step 3, Scheme 2). As previously reported, this neutral radical can react with highly electrophilic **2** through a homolytic aromatic substitution (Step 3, Scheme 2).[67] Then, a second SET from the excited state of a proximal **PD2-CD** (−2.44 V) to the activated complex (Step 4, Scheme 2) may reduce the resulting radical σ-complex by eliminating

the chlorine (as Cl^-) and yielding the desired α-heteroarylation product (Step 5, Scheme 2). Therefore, the only anticipated by-product of this reaction is HCl.

Table 1. Assessment of multiple α-heteroarylation conditions.

Entry	*Catalyst*	*NaOAc (equiv.)*	*Reaction time (hrs)*[a]	*Yield (%)*[b]
1	ZnO NW|PD2-CD	1.0	4	32
2	ZnO NW|PD2-CD	2.0	10	82
3	ZnO NW|PD2-CD	1.0	12	60
4	ZnO NW|PD2-CD	1.0	24	82
5	ZnO NW|PD2-CD	2.0	24	97
6	PD2-CD dispersion	1.0	4	8
7	PD2-CD dispersion	1.0	24	56
8	ZnO NWs	1.0	24	50
9	ZnO NW|PD2-CD[c]	1.0	24	0

[a] All reactions were performed with 10 equiv. of water in 0.25 M dimethylacetamide at room temperature under white light irradiation. [b] The yield was calculated from an average of three reactions with 1,3,5-trimethoxybenzene as an internal standard for ^{1}H NMR. [c] Reaction performed in the dark.

The crude product of the reaction was extracted with ethyl acetate, purified, and isolated for characterization by column chromatography following the procedures detailed in the Supplementary Information. The isolated product was characterized, and determined to be the desired 2-(1-phenylpyrrolidin-2-yl)benzo[d]thiazole (Scheme 1; **3**), through ^{1}H NMR (Figure S15), ^{13}C NMR (Figure S16) and high-resolution mass spectrometry (HRMS, Figure S17). The crude reaction yield was calculated through ^{1}H NMR using 1,3,5-trimethoxybenzene as an internal standard. It is worth noting the yield of the control experiments where the **PD2-CD** dispersions are expected to generate the product owing to their excited state redox potentials

which suffice to catalyze the reaction. When compared to the **ZnO NW|PD2-CD** films, we still observed a lower yield for the unsupported **PD2-CDs** (8% after 4 hrs) due to a lack of an electron sink and stabilizer. In contrast, the bare ZnO NWs somewhat unexpectedly produced a yield of 50% (24 hrs) that may be attributed to formation of a radical ion pair via reductive quenching of the excited state of **2** by **1** (we note **2** absorbs light at the blue edge of the visible spectrum, λ_{ex} = 390–400 nm, Figure S18, enabling excitation by the white light LEDs). From our work, it is unclear whether electron injection into the ZnO NWs occurs from this radical pair or prior to its formation, however we anticipate that either process will enable entrance into the proposed catalytic cycle. Overall, our observed yields approach or surpass those previously reported for this transformation with the molecular photocatalyst $[Ir(ppy)_2(dtbbpy)][PF_6]$.[67]

Conclusion

We have successfully engineered a heterogeneous catalytic photoelectrode from Earth-abundant elements for the α-heteroarylation of 1-phenylpyrrolidine (**1**) with 2-chlorobenzothiazole (**2**) at room temperature to produce 2-(1-phenylpyrrolidin-2-yl)benzo[d]thiazole (**3**). The photoelectrode makes use of ZnO NWs grown on an FTO substrate as a support and electron sink and is further sensitized to visible light by the attachment of **PD2-CDs** onto the surface. The energetics of the system at the heterojunctions were investigated and compared, and it was determined that the energy levels were aligned in a way that maximizes the efficiency of photocatalysis by promoting forward electron transfer. From optical spectroscopy and electrochemistry investigations, the mechanism for the electron transfer at the ZnO/CD interface was also explored to get insight on the role of **PD2-CDs** in photocatalytic processes, a subject that is usually obviated in the field. It was concluded that these specific CDs participate in both the oxidation and reduction reactions and thus, are a crucial component of the

photocatalysis. Also, the presence of the ZnO NWs was determined to be necessary to promote the flow of electrons from and into the **PD2-CDs** and to achieve higher reaction yields.

The system described in this work can surpass the performance of precious metal-containing photocatalysts and is built from inexpensive elements having the characteristics of a heterogeneous photocatalyst. Therefore, it may render itself more practical and advantageous than classical molecular systems. This work establishes a proof-of-concept to elucidate the underlying charge transfer mechanisms on the interaction between CDs and semiconductor nanostructures. We foresee the engineering of similar CD-based photocatalysts to produce value-added chemicals through solar-to-chemical energy conversion based on the study of the energetics of the components coming together, and work to optimize the current system is underway in our laboratory.

ASSOCIATED CONTENT

Supporting Information. Procedures for the formation of ZnO nanoparticles, optimization of ZnO nanowire growth, synthesis of carbon dots, electrochemistry, electron microscopy, and X-ray photoelectron spectroscopy data is available in the Supporting Information. This material is available free of charge via the Internet at http://pubs.acs.org.

AUTHOR INFORMATION

Corresponding Author

* E-mail: marek.majewski@concordia.ca (M.B.M.)

Author Contributions

F.Y. carried out the experimental work. J.M. first prepared the RCDs and PD2-CDs. The manuscript was written through contributions of all authors. All authors have given approval to the final version of the manuscript.

ACKNOWLEDGMENT

The authors thank the Natural Sciences and Engineering Research Council of Canada (NSERC), the Fonds de Recherche du Québec – Nature et technologies (FRQNT) and the Quebec Centre for Advanced Materials (QCAM) for financial support. F.Y. thanks Concordia University for research support under a Graduate Scholarship in Natural Sciences and Engineering Research (CGS NSER) award. SEM work was carried out by Hudson Bicalho at the Federal University of Minas Gerais. XPS analysis was performed at McGill University (MIAM) with the assistance of Dr. Lihong Shang. TEM work was performed at McGill University (MILab) in the Chemistry Characterization facility with the assistance of Mohini Ramkaran and at Polytechnique Montreal in the Centre for Characterization and Microscopy of Materials (CM2) with the assistance of Jean-Philippe Masse. DRS and profilometry was performed at Université de Montréal (LAMP lab) with the assistance of Dr. Daniel Chartrand. Mass spectrometry work was done at the Centre for Biological Applications of Mass Spectrometry (CBAMS) with the assistance of Alain Tessier. The authors also thank Jian Tian Liu and Zujhar Singh for their insightful discussions and Daniela Aguayo for her assistance with the TOC artwork.

REFERENCES

1. Sanzone, A.; Mattiello, S.; Garavaglia, G. M.; Calascibetta, A. M.; Ceriani, C.; Sassi, M.; Beverina, L., Efficient synthesis of organic semiconductors by Suzuki–Miyaura coupling in an aromatic micellar medium. *Green Chem.* **2019,** *21* (16), 4400-4405.
2. Jiang, W.; Li, Y.; Wang, Z., Heteroarenes as high performance organic semiconductors. *Chem. Soc. Rev.* **2013,** *42* (14), 6113-6127.

3. Mohanty, A. D.; Lee, Y.-B.; Zhu, L.; Hickner, M. A.; Bae, C., Anion Exchange Fuel Cell Membranes Prepared from C–H Borylation and Suzuki Coupling Reactions. *Macromolecules* **2014,** *47* (6), 1973-1980.
4. He, C.; Hao, J.; Xu, H.; Mo, Y.; Liu, H.; Han, J.; Lei, A., Heteroaromatic Imidazo[1,2-a]pyridines Synthesis from C–H/N–H Oxidative Cross-Coupling/Cyclization. *Chem. Commun.* **2012,** *48* (90), 11073-11075.
5. Colmenares, J. C.; Luque, R., Heterogeneous Photocatalytic Nanomaterials: Prospects and Challenges in Selective Transformations of Biomass-Derived Compounds. *Chem. Soc. Rev.* **2014,** *43* (3), 765-778.
6. Artero, V.; Fontecave, M., Solar Fuels Generation and Molecular Systems: Is it Homogeneous or Heterogeneous Catalysis? *Chem. Soc. Rev.* **2013,** *42* (6), 2338-2356.
7. Hooshmand, S. E.; Heidari, B.; Sedghi, R.; Varma, R. S., Recent Advances in the Suzuki–Miyaura Cross-Coupling Reaction Using Efficient Catalysts in Eco-Friendly Media. *Green Chem.* **2019,** *21* (3), 381-405.
8. Pethő, B.; Vangel, D.; Csenki, J. T.; Zwillinger, M.; Novák, Z., Palladium Catalyzed Chloroethoxylation of Aromatic and Heteroaromatic Chlorides: an Orthogonal Functionalization of a Chloroethoxy Linker. *Org. Biomol. Chem.* **2018,** *16* (26), 4895-4899.
9. Jin, B.; Gallou, F.; Reilly, J.; Lipshutz, B. H., ppm Pd-Catalyzed, Cu-Free Sonogashira Couplings in Water Using Commercially Available Catalyst Precursors. *Chem. Sci.* **2019,** *10* (12), 3481-3485.
10. Long, R.; Huang, H.; Li, Y.; Song, L.; Xiong, Y., Palladium-Based Nanomaterials: A Platform to Produce Reactive Oxygen Species for Catalyzing Oxidation Reactions. *Adv. Mater.* **2015,** *27* (44), 7025-7042.
11. Zhang, Z.; Richrath, R. B.; Gansäuer, A., Merging Catalysis in Single Electron Steps with Photoredox Catalysis—Efficient and Sustainable Radical Chemistry. *ACS Catal.* **2019,** *9* (4), 3208-3212.
12. Stache, E. E.; Ertel, A. B.; Rovis, T.; Doyle, A. G., Generation of Phosphoranyl Radicals via Photoredox Catalysis Enables Voltage–Independent Activation of Strong C–O Bonds. *ACS Catal.* **2018,** *8* (12), 11134-11139.
13. Cai, Y.; Tang, Y.; Fan, L.; Lefebvre, Q.; Hou, H.; Rueping, M., Heterogeneous Visible-Light Photoredox Catalysis with Graphitic Carbon Nitride for α-Aminoalkyl Radical Additions, Allylations, and Heteroarylations. *ACS Catal.* **2018,** *8* (10), 9471-9476.
14. Ghogare, A. A.; Greer, A., Using Singlet Oxygen to Synthesize Natural Products and Drugs. *Chem. Rev.* **2016,** *116* (17), 9994-10034.
15. Rehman, S.; Ullah, R.; Butt, A. M.; Gohar, N. D., Strategies of Making TiO2 and ZnO Visible Light Active. *J. Hazard. Mater.* **2009,** *170* (2-3), 560-9.
16. Camussi, I.; Mannucci, B.; Speltini, A.; Profumo, A.; Milanese, C.; Malavasi, L.; Quadrelli, P., g-C3N4 - Singlet Oxygen Made Easy for Organic Synthesis: Scope and Limitations. *ACS Sustainable Chem. Eng.* **2019,** *7* (9), 8176-8182.
17. Xu, X.; Luo, F.; Tang, W.; Hu, J.; Zeng, H.; Zhou, Y., Enriching Hot Electrons via NIR-Photon-Excited Plasmon in WS2@Cu Hybrids for Full-Spectrum Solar Hydrogen Evolution. *Adv. Funct. Mater.* **2018,** *28* (43), 1804055.
18. Yuan, J.; Wen, J.; Gao, Q.; Chen, S.; Li, J.; Li, X.; Fang, Y., Amorphous Co3O4 Modified CdS Nanorods with Enhanced Visible-Light Photocatalytic H2-Production Activity. *Dalton Trans.* **2015,** *44* (4), 1680-1689.

19. Rand, B. P.; Burk, D. P.; Forrest, S. R., Offset Energies at Organic Semiconductor Heterojunctions and their Influence on the Open-Circuit Voltage of Thin-Film Solar Cells. *Phys. Rev. B* **2007,** *75* (11), 115327.
20. Li, X.; Yu, J.; Jaroniec, M., Hierarchical Photocatalysts. *Chem. Soc. Rev.* **2016,** *45* (9), 2603-2636.
21. Greene, L. E.; Yuhas, B. D.; Law, M.; Zitoun, D.; Yang, P., Solution-Grown Zinc Oxide Nanowires. *Inorg. Chem.* **2006,** *45* (19), 7535-7543.
22. Osterloh, F. E., Inorganic Nanostructures for Photoelectrochemical and Photocatalytic Water Splitting. *Chem. Soc. Rev.* **2013,** *42* (6), 2294-2320.
23. Zhang, Q.; Dandeneau, C. S.; Zhou, X.; Cao, G., ZnO Nanostructures for Dye-Sensitized Solar Cells. *Adv. Mater.* **2009,** *21* (41), 4087-4108.
24. Bora, T.; Zoepfl, D.; Dutta, J., Importance of Plasmonic Heating on Visible Light Driven Photocatalysis of Gold Nanoparticle Decorated Zinc Oxide Nanorods. *Sci. Rep.* **2016,** *6*, 26913.
25. Šutka, A.; Käämbre, T.; Pärna, R.; Juhnevica, I.; Maiorov, M.; Joost, U.; Kisand, V., Co Doped ZnO Nanowires as Visible Light Photocatalysts. *Solid State Sci.* **2016,** *56*, 54-62.
26. Unalan, H. E.; Wei, D.; Suzuki, K.; Dalal, S.; Hiralal, P.; Matsumoto, H.; Imaizumi, S.; Minagawa, M.; Tanioka, A.; Flewitt, A. J.; Milne, W. I.; Amaratunga, G. A. J., Photoelectrochemical cell using dye sensitized zinc oxide nanowires grown on carbon fibers. *Appl. Phys. Lett.* **2008,** *93* (13), 133116.
27. Kadi, M. W.; McKinney, D.; Mohamed, R. M.; Mkhalid, I. A.; Sigmund, W., Fluorine Doped Zinc Oxide Nanowires: Enhanced Photocatalysts Degrade Malachite Green Dye Under Visible Light Conditions. *Ceram. Int.* **2016,** *42* (4), 4672-4678.
28. Guo, C. X.; Dong, Y.; Yang, H. B.; Li, C. M., Graphene Quantum Dots as a Green Sensitizer to Functionalize ZnO Nanowire Arrays on F-Doped SnO2 Glass for Enhanced Photoelectrochemical Water Splitting. *Adv. Energy Mater.* **2013,** *3* (8), 997-1003.
29. Lee, C.-P.; Chou, C.-Y.; Chen, C.-Y.; Yeh, M.-H.; Lin, L.-Y.; Vittal, R.; Wu, C.-G.; Ho, K.-C., Zinc Oxide-Based Dye-Sensitized Solar Cells with a Ruthenium Dye Containing an Alkyl Bithiophene Group. *J. Power Sources* **2014,** *246*, 1-9.
30. Zhang, X.; Cappel, U. B.; Jia, D.; Zhou, Q.; Du, J.; Sloboda, T.; Svanström, S.; Johansson, F. O. L.; Lindblad, A.; Giangrisostomi, E.; Ovsyannikov, R.; Liu, J.; Rensmo, H.; Gardner, J. M.; Johansson, E. M. J., Probing and Controlling Surface Passivation of PbS Quantum Dot Solid for Improved Performance of Infrared Absorbing Solar Cells. *Chem. Mater.* **2019,** *31* (11), 4081-4091.
31. Briscoe, J.; Marinovic, A.; Sevilla, M.; Dunn, S.; Titirici, M., Biomass-Derived Carbon Quantum Dot Sensitizers for Solid-State Nanostructured Solar Cells. *Angew. Chem. Int. Ed.* **2015,** *54* (15), 4463-4468.
32. Macina, A.; de Medeiros, T. V.; Naccache, R., A carbon dot-catalyzed transesterification reaction for the production of biodiesel. *J. Mater. Chem. A* **2019,** *7* (41), 23794-23802.
33. Yu, H.; Shi, R.; Zhao, Y.; Waterhouse, G. I. N.; Wu, L.-Z.; Tung, C.-H.; Zhang, T., Smart Utilization of Carbon Dots in Semiconductor Photocatalysis. *Adv. Mater.* **2016,** *28* (43), 9454-9477.
34. Manioudakis, J.; Victoria, F.; Thompson, C. A.; Brown, L.; Movsum, M.; Lucifero, R.; Naccache, R., Effects of Nitrogen-Doping on the Photophysical Properties of Carbon Dots. *J. Mater. Chem. C* **2019,** *7* (4), 853-862.

35. Wang, R.; Lu, K.-Q.; Tang, Z.-R.; Xu, Y.-J., Recent progress in carbon quantum dots: synthesis, properties and applications in photocatalysis. *J. Mater. Chem. A* **2017,** *5* (8), 3717-3734.
36. Hazarika, D.; Karak, N., Photocatalytic Degradation of Organic Contaminants Under Solar Light Using Carbon Dot/Titanium Dioxide Nanohybrid, Obtained Through a Facile Approach. *Appl. Surf. Sci.* **2016,** *376*, 276-285.
37. Xu, X.; Bao, Z.; Tang, W.; Wu, H.; Pan, J.; Hu, J.; Zeng, H., Surface States Engineering Carbon dots as Multi-Band Light Active Sensitizers for ZnO Nanowire Array Photoanode to Boost Solar Water Splitting. *Carbon* **2017,** *121*, 201-208.
38. Hutton, G. A. M.; Reuillard, B.; Martindale, B. C. M.; Caputo, C. A.; Lockwood, C. W. J.; Butt, J. N.; Reisner, E., Carbon Dots as Versatile Photosensitizers for Solar-Driven Catalysis with Redox Enzymes. *J. Am. Chem. Soc.* **2016,** *138* (51), 16722-16730.
39. Omer, K. M.; Mohammad, N. N.; Baban, S. O., Up-Conversion Fluorescence of Phosphorous and Nitrogen Co-Doped Carbon Quantum Dots (CDs) Coupled with Weak LED Light Source for Full-Spectrum Driven Photocatalytic Degradation via ZnO-CDs Nanocomposites. *Catal. Lett.* **2018,** *148* (9), 2746-2755.
40. Zhu, M.; Deng, X.; Lin, X.; Zhang, L.; Zhang, W.; Lv, Y.; Pan, J., The carbon quantum dots modified ZnO/TiO2 nanotube heterojunction and its visible light photocatalysis enhancement. *J. Mater. Sci.: Mater. Electron.* **2018,** *29* (13), 11449-11456.
41. Barman, M. K.; Mitra, P.; Bera, R.; Das, S.; Pramanik, A.; Parta, A., An Efficient Charge Separation and Photocurrent Generation in the Carbon Dot–Zinc Oxide Nanoparticle Composite. *Nanoscale* **2017,** *9* (20), 6791-6799.
42. Suzuki, K.; Malfatti, L.; Carboni, D.; Loche, D.; Casula, M.; Moretto, A.; Maggini, M.; Takahashi, M.; Innocenzi, P., Energy Transfer Induced by Carbon Quantum Dots in Porous Zinc Oxide Nanocomposite Films. *J. Phys. Chem. C* **2015,** *119* (5), 2837-2843.
43. Low, J.; Yu, J.; Jaroniec, M.; Wageh, S.; Al-Ghamdi, A. A., Heterojunction Photocatalysts. *Adv. Mater.* **2017,** *29* (20), 1601694.
44. Wang, M.; Cai, L.; Wang, Y.; Zhou, F.; Xu, K.; Tao, X.; Chai, Y., Graphene-Draped Semiconductors for Enhanced Photocorrosion Resistance and Photocatalytic Properties. *J. Am. Chem. Soc.* **2017,** *139* (11), 4144-4151.
45. Lim, S. Y.; Shen, W.; Gao, Z., Carbon Quantum Dots and Their Applications. *Chem. Soc. Rev.* **2015,** *44* (1), 362-381.
46. Omri, K.; Alyamani, A.; El Mir, L., Surface morphology, microstructure and electrical properties of Ca-doped ZnO thin films. *J. Mater. Sci.: Mater. Electron.* **2019,** *30* (17), 16606-16612.
47. Tian, Z. R.; Voigt, J. A.; Liu, J.; McKenzie, B.; McDermott, M. J.; Rodriguez, M. A.; Konishi, H.; Xu, H., Complex and Oriented ZnO Nanostructures. *Nature Materials* **2003,** *2* (12), 821-826.
48. Dong, Y.; Pang, H.; Yang, H. B.; Guo, C.; Shao, J.; Chi, Y.; Li, C. M.; Yu, T., Carbon-Based Dots Co-doped with Nitrogen and Sulfur for High Quantum Yield and Excitation-Independent Emission. *Angew. Chem. Int. Ed.* **2013,** *52* (30), 7800-7804.
49. Sahu, S.; Behera, B.; Maiti, T. K.; Mohapatra, S., Simple One-Step Synthesis of Highly Luminescent Carbon Dots from Orange Juice: Application as Excellent Bio-Imaging Agents. *Chem. Commun.* **2012,** *48* (70), 8835-8837.

50. Song, Y.; Zhu, S.; Zhang, S.; Fu, Y.; Wang, L.; Zhao, X.; Yang, B., Investigation from chemical structure to photoluminescent mechanism: a type of carbon dots from the pyrolysis of citric acid and an amine. *J. Mater. Chem. C* **2015,** *3* (23), 5976-5984.
51. Wang, W.; Wang, B.; Embrechts, H.; Damm, C.; Cadranel, A.; Strauss, V.; Distaso, M.; Hinterberger, V.; Guldi, D. M.; Peukert, W., Shedding light on the effective fluorophore structure of high fluorescence quantum yield carbon nanodots. *RSC Adv.* **2017,** *7* (40), 24771-24780.
52. Pan, L.; Sun, S.; Zhang, L.; Jiang, K.; Lin, H., Near-Infrared Emissive Carbon Dots for Two-Photon Fluorescence Bioimaging. *Nanoscale* **2016,** *8* (39), 17350-17356.
53. Wang, Y.; Wöll, C., IR Spectroscopic Investigations of Chemical and Photochemical Reactions on Metal Oxides: Bridging the Materials Gap. *Chem. Soc. Rev.* **2017,** *46* (7), 1875-1932.
54. Dominguez, A.; Lorke, M.; Schoenhalz, A. L.; Rosa, A. L.; Frauenheim, T.; Rocha, A. R.; Dalpian, G. M., First principles investigations on the electronic structure of anchor groups on ZnO nanowires and surfaces. *J. Appl. Phys.* **2014,** *115* (20), 203720.
55. Moreira, N. H.; Rosa, A. L. d.; Frauenheim, T., Covalent functionalization of ZnO surfaces: A density functional tight binding study. *Appl. Phys. Lett.* **2009,** *94* (19), 193109.
56. Martsinovich, N.; Troisi, A., Theoretical studies of dye-sensitised solar cells: from electronic structure to elementary processes. *Energy Environ. Sci.* **2011,** *4* (11), 4473-4495.
57. Lu, Q.; Yu, Y.; Ma, Q.; Chen, B.; Zhang, H., 2D Transition-Metal-Dichalcogenide-Nanosheet-Based Composites for Photocatalytic and Electrocatalytic Hydrogen Evolution Reactions. *Adv. Mater.* **2016,** *28* (10), 1917-1933.
58. Yarur, F.; Macairan, J.-R.; Naccache, R., Ratiometric Detection of Heavy Metal Ions Using Fluorescent Carbon Dots. *Environ. Sci. Nano* **2019,** *6* (4), 1121-1130.
59. Shen, J.; Zhu, Y.; Yang, X.; Zong, J.; Zhang, J.; Li, C., One-Pot Hydrothermal Synthesis of Graphene Quantum Dots Surface-Passivated by Polyethylene Glycol and Their Photoelectric Conversion Under Near-Infrared Light. *New J. Chem.* **2012,** *36* (1), 97-101.
60. Ding, H.; Yu, S.-B.; Wei, J.-S.; Xiong, H.-M., Full-Color Light-Emitting Carbon Dots with a Surface-State-Controlled Luminescence Mechanism. *ACS Nano* **2016,** *10* (1), 484-491.
61. Pal, A.; Ghosh, I.; Sapra, S.; König, B., Quantum Dots in Visible-Light Photoredox Catalysis: Reductive Dehalogenations and C–H Arylation Reactions Using Aryl Bromides. *Chem. Mater.* **2017,** *29* (12), 5225-5231.
62. Sakai, J.; Miura, I.; Shibata, M.; Yonekura, N.; Hiyoshi, H.; Takagaki, M.; Nagayama, K., Development of a New Fungicide, Benthiavalicarb-Isopropyl. *J. Pestic. Sci.* **2010,** *35* (4), 488-489.
63. Solanki, P. V.; Uppelli, S. B.; Patil, R. B.; Dhokrat, P. A.; Bembalkar, S. R.; Mathad, V. T., Facile Synthesis of Dabigatran Etexilate Mesylate, an Anticoagulant Drug, Using a Novel Synthon, N-Hexyl-4-nitrophenyl Carbonate. *ACS Omega* **2018,** *3* (5), 5744-5753.
64. Donawho, C. K.; Luo, Y.; Luo, Y.; Penning, T. D.; Bauch, J. L.; Bouska, J. J.; Bontcheva-Diaz, V. D.; Cox, B. F.; DeWeese, T. L.; Dillehay, L. E.; Ferguson, D. C.; Ghoreishi-Haack, N. S.; Grimm, D. R.; Guan, R.; Han, E. K.; Holley-Shanks, R. R.; Hristov, B.; Idler, K. B.; Jarvis, K.; Johnson, E. F.; Kleinberg, L. R.; Klinghofer, V.; Lasko, L. M.; Liu, X.; Marsh, K. C.; McGonigal, T. P.; Meulbroek, J. A.; Olson, A. M.; Palma, J. P.; Rodriguez, L. E.; Shi, Y.; Stavropoulos, J. A.; Tsurutani, A. C.; Zhu, G.-D.; Rosenberg, S. H.; Giranda, V. L.; Frost, D. J., ABT-888, an Orally Active Poly(ADP-Ribose) Polymerase Inhibitor

that Potentiates DNA-Damaging Agents in Preclinical Tumor Models. *Clin. Cancer Res.* **2007,** *13* (9), 2728-2737.
65. Hauel, N. H.; Nar, H.; Priepke, H.; Ries, U.; Stassen, J.-M.; Wienen, W., Structure-Based Design of Novel Potent Nonpeptide Thrombin Inhibitors. *J. Med. Chem.* **2002,** *45* (9), 1757-1766.
66. Reuveni, M., Activity of the New Fungicide Benthiavalicarb Against Plasmopara viticola and its Efficacy in Controlling Downy Mildew in Grapevines. *Eur. J. Plant Pathol.* **2003,** *109* (3), 243-251.
67. Prier, C. K.; MacMillan, D. W. C., Amine α-Heteroarylation Via Photoredox Catalysis: a Homolytic Aromatic Substitution Pathway. *Chem. Sci.* **2014,** *5* (11), 4173-4178.
68. McNally, A.; Prier, C. K.; MacMillan, D. W. C., Discovery of an α-Amino C–H Arylation Reaction Using the Strategy of Accelerated Serendipity. *Science* **2011,** *334* (6059), 1114-1117.
69. Zhang, H.; Zong, R.; Zhu, Y., Photocorrosion Inhibition and Photoactivity Enhancement for Zinc Oxide via Hybridization with Monolayer Polyaniline. *J. Phys. Chem. C* **2009,** *113* (11), 4605-4611.
70. Arnaut, L.; Formosinho, S.; Burrows, H., 4 - Reaction Order and Rate Constants. In *Chemical Kinetics*, Arnaut, L.; Formosinho, S.; Burrows, H., Eds. Elsevier: Amsterdam, 2007; pp 77-113.

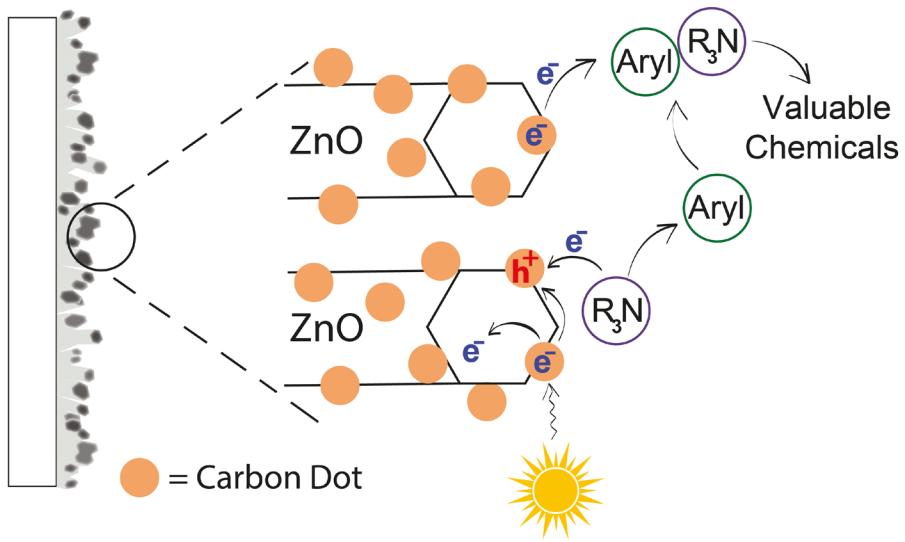

Table of Contents Artwork